One-pot solvothermal synthesis of dual-phase titanate/titania nanoparticles and their adsorption and photocatalytic performances

Cheng, Yu Hua; Gong, Dangguo; Tang, Yuxin; Ho, Jeffery Weng Chye; Tay, Yee Yan; Lau, Wei Siew; Wijaya, Olivia; Lim, Jiexiang; Chen, Zhong

2013

Cheng, Y. H., Gong, D., Tang, Y., Ho, J. W. C., Tay, Y. Y., Lau, W. S., et al. (2014). One-pot solvothermal synthesis of dual-phase titanate/titania nanoparticles and their adsorption and photocatalytic performances. Journal of solid state chemistry, 214, 67-73.

https://hdl.handle.net/10356/102897

https://doi.org/10.1016/j.jssc.2013.10.036

One-pot Solvothermal Synthesis of Dual-phase Titanate/titania Nanoparticles and Their Adsorption and Photocatalytic Performances

Yu Hua Cheng, Dangguo Gong, Yuxin Tang, Jeffery Weng Chye Ho, Yee Yan Tay, Wei Siew Lau, Olivia Wijaya, Jiexiang Lim, Zhong Chen*

School of Materials Science and Engineering, Nanyang Technological University,

50 Nanyang Avenue, Singapore 639798

Abstract:

Dual phase titanate/titania nanoparticles undergo phase transformation gradually with the increase of solvothermal synthesis temperature from 100 °C to 200 °C, and eventually are fully transformed into anatase TiO_2. The crystal structure change results in the changes of optical absorption, sensitizer/dopant formation and surface area of the materials and finally affect the overall photocatalytic activity. Reactions under dark and light have been conducted to distinguish the contributions of surface adsorption from light degradation. The sample synthesized at 160 °C (S160) shows the best performances for both adsorption under dark and photo-degradation of methylene blue (MB) under visible light irradiation. The adsorption mechanism for S160 is determined as monolayer adsorption based on the adsorption isotherm test under dark condition, and an impressive adsorption capacity of 162.19 mg/g is achieved. For the photocatalytic application, this sample at 0.1g/L loading is also able to degrade 20 ppm MB within 6 hours under the visible light (> 420 nm) condition.

* Email: aszchen@ntu.edu.sg (Z. C).

Tel.: +65 6790 4256; Fax: +65 6790 9081.

Keywords: solvothermal synthesis; photocatalyst; titanate; titania; visible light activity; adsorption

1. Introduction

Environmental contamination is one of the great challenges we are facing nowadays [1-4]. Photocatalysis is a promising technology making use of solar energy to break down toxic organic pollutants into neutral CO_2 and H_2O, which doesn't require extra chemical and energy input [5, 6]. An ideal photocatalyst needs to fulfill several criteria [7-13]: (1) effective absorption of solar energy by extending its absorption range to visible light; (2) efficient charge separation to prevent photogenerated electron-hole recombination; (3) high surface area allowing easy adsorption of reactants and providing more reactive sites; (4) chemically stable under light irradiation, robust against photo-corrosion and low in toxicity. To date, the full potential of photocatalysis in practical applications has not been reached as these challenges have yet to be overcome. Most stable photocatalytic materials studied so far such as TiO_2 and $SrTiO_3$, are capable of absorbing UV light that only covers 5% of solar spectrum [14], while some visible light active photocatalysts, such as CdS, undergo photo-corrosion during irradiation [15-18]. In addition, these materials often have poor surface adsorption for organic species. Much work has been focused on extending the light absorption of TiO_2 related materials into the visible light range but the visible light adsorption and photocatalytic performance is not so ideal [19].

Titanates are a new family of photocatalytic materials that were introduced in the late 1990s and the research in this work only grew active in the recent years [16, 20-22]. They combine the properties of conventional TiO_2 with properties of layered materials that make them favorable for ion exchange [23, 24]. A unique property of titanates is their strong physical adsorption

capacity. Nanostructured titanates possess large surface areas and can adsorb organic species such as dyes on their surfaces [25-28]. Good interfacial contact between photocatalyst and adsorbed species enhances electron-hole interaction and reduces the possibility of charge recombination. Despite these advantages, titanates are responsive only to UV light as they have been reported to possess wide band-gaps between 3.4 to 3.8 eV [16, 29]. In addition, the synthesis of such materials often involves complex processes which require intense acidic/alkaline conditions and high temperatures [21, 22, 30, 31].

We have previously reported a unique dual phase photocatalyst that displays excellent degradation of methylene blue and phenol under visible light [32, 33]. The material comprises of a hydrated layered titanate and anatase TiO_2 with visible light sensitivity due to nitrogen doping and surface sensitization. However, little was known about the influence of synthesis condition on the phase transformation, crystallinity and performance of this class of mixed phase TiO_2-based materials. Particularly, there has been no systematic investigation on the differentiation between surface adsorption and photocatalytic degradation. In this paper, we explore the variation of synthesis temperature and its influence on crystal structure, optical absorption, dopant formation and the specific surface area. In particular, this temperature study allows an observation of phase transition across the samples and its effect on overall photocatalytic activity. Importantly, reactions under dark and light were conducted to distinguish the contributions of surface adsorption from light degradation. The adsorption isotherm and kinetics of the best performing material were investigated to understand the adsorption mechanism. The visible light photocatalytic degradation kinetics was also studied.

2. Experimental

2.1 Sample preparation

Chemicals and materials used for synthesis were titanium isopropoxide [Ti $(OC_3H_7)_4$, 99.5%, Aldrich], ethanol [technical grade, 95%], acetylacetone [$C_5H_8O_2$, 99.5%, Fluka], triethylamine [$N(CH_2CH_3)_3$, 99.5%, Aldrich] and deionized water. Ethanol and acetylacetone (ACAC) were mixed in molar proportion of 20: 1. Next, titanium isopropoxide (TI) and triethylamine (TE) were added simultaneously dropwise in molar ratio of 1:4. Lastly, 3 mol of deionized water were added and the mixture was allowed to stir for 30 minutes. Following this, 50 mL of this clear yellow solution was measured into a 125 mL capacity stainless steel autoclave for hydrothermal reaction. The autoclave was then heated in an ambient oven for duration of 3 hours at temperatures varying from 100 to 200 ºC. The as-prepared samples were labeled as SX, where X denotes the synthesis temperature. The autoclave was cooled under ambient conditions. Thereafter, the gel was dried in an oven at 80 ºC. The extracted powder was cleaned repeatedly with ethanol and deionized water via centrifuging process to remove traces of organic waste. Lastly, the powder was re-dried in ambient oven at 80 ºC and collected.

2.2 Materials characterization

X-ray diffraction was used to study the crystal structure and phase transition across the increasing synthesis temperatures. The XRD patterns of the powders were recorded using a Shimadzu LabX-6000 diffractometer of CuKα radiation (λ = 0.15418 nm) equipped with a secondary graphite monochromator. A step size of 0.02º over 2θ ranging from 5 to 80º was used with scanning rate set at 0.2º per minute. Optical absorption of the bulk powders were measured on Perkin Elmer Lambda 900 UV-Visible spectrometer in diffuse reflectance spectroscopy mode over the spectral range of 200 - 800 nm. The nature of dopant species and bond integrity across

the samples were analyzed using X- ray photoelectron spectroscopy, XPS (Kratos Axis ULTRA). Specific surface area and pore size was determined using a Micromeritics ASAP 2020 surface analyzer based on the Brunauer Emmett Teller, BET theory. The samples were outgassed under vacuum and heated to 100 ºC. JEOL 2100-F transmission electron microscopy (TEM) with a field emission gun was used to observe the morphology of the synthesized samples. The accelerating voltage was 200 kV. The synthesized powders were dispersed in ethanol and ultrasonicated for 5 min. The dispersion was then dropped onto a holey-carbon-copper grid for imaging.

2.3 Adsorption and photocatalytic degradation of methylene blue under visible light

Methylene blue (MB) dye was chosen as primary candidate for photocatalytic degradation activity of the prepared powders in order to study both adsorption and degradation effects. Solutions of the dye were prepared by mixing with deionized water at 20 ppm concentration. 10 mg of photocatalyst powder was dispersed in 100 mL of each MB solution. An adsorption isotherm test was carried out by varying concentrations of methylene blue from 5 to 50 ppm. For each test, 10 mg of adsorbent was added to 100 mL of MB solution. The equilibrium concentration was measured after adsorption saturation of each test was reached.

Control experiments were performed for mixtures in the dark as well as blank MB solutions under light irradiation. In addition, reference photocatalyst powder Degussa P25 TiO_2 was also tested as a platform for comparison of photocatalytic activity. The irradiation source was a 450W Newport Xenon Arc lamp with spectral range from 200- 2500 nm. A short wave light filter was used to cut off the transmission below 420 nm. A cooling water filter was also attached to block IR-rays and prevent excessive heating. MB suspension was placed directly

under the light source so that the irradiation was uniform over the surface of the solution. During the experiment, the suspension was kept under stirring to ensure an aerobic environment for complete dye mineralization reaction [34]. Samples were taken at regular time intervals and underwent centrifuging. The spectral intensity measurements of the degraded dye were performed on a Shimadzu 2500 UV- Visible spectrometer.

3. Results and discussion

3.1 XRD and TEM analyses

Figure 1 presents the XRD patterns of the samples synthesized with varying hydrothermal temperatures from 100 to 200 °C. Across curves (a) to (c), broad peaks with relative low intensities appear. Samples S100, S130 and S160 display low angle diffraction at 8.56º, 17.01º and 26.39º. These peaks correspond to a layered hydrogen titanate $H_2Ti_3O_7 \cdot xH_2O$. We shared in previous report about the crystal structure of this titanate in detail [33]. In that report, S160 was found to be a dual phase structure containing titanate and anatase phase in approximately 50:50 weight ratio. It is believed that S100 and S130 possessed dual phases where titanate existed in greater proportions at lower temperatures albeit having poorer crystallinity. As the hydrothermal temperature increases, the peaks grow sharper; an indication of improving crystallinity and nano-particle growth. Additional peaks at 37.78º, 48.77º and 62.86º also emerged in samples S130 (curve b) and S160 (curve c). Curve (d) of Figure 1 shows the crystal structure underwent phase changes as the hydrothermal temperature increased to 170 ºC for sample S170. The first two low angle peaks at 8.56º and 17.01º decreased and the third peak at 26.39º sharpened and shifted to 25.28º. Other distinct peaks also emerged. These peaks can be perfectly indexed to the well-known anatase titanium oxide structure (PDF card #21-1272)

having tetragonal system and lattice constants a = 0.3785 nm, c = 0.9614 nm. S170 is likely to assimilate a mixture of intermediate titanate phase evolving into anatase. Finally, in curve (e), the sample evolves completely into anatase at a temperature of 200 ºC.

TEM images in Figure 2 shows that the S100 sample consists of agglomerated nanoparticles with numerous tiny pores within the agglomeration. With increased synthesis temperature, S160 shows clear cubic particles averaging 20 nm in size with intra-granular pores with a size around 3.5 nm. At 200 °C, individual solid cubic particles are clearly differentiable (S200, Figure 2c), but the particle size has not increased much as compared with S160. With the increase of synthesis temperature and increased anatase content in the dual-phase mixture, there is a clear trend that the crytallinity increases, and the morphology gradually changes to the anatase-dominant cubic shape. The number of pores and their size decrease steadily, probably due to the faster ripening process at higher synthesis temperatures.

3.2 UV-Vis Diffuse Reflectance Spectroscopy

Figure 3 displays a visual comparison of the as-synthesized powders in the original temperature study set. From observation, S100, S130 and S160 appears to be a similar shade of deep yellowish orange which is a characteristic feature of N-sensitized samples [35, 36]. S170 appeared brownish in color and S200 was a light shade of beige. The changes in color of the powders point towards a shift in light absorption as shown in diffuse reflectance spectroscopy results in Figure 3. S100, S130 and S160 show comparable optical absorption curves that extends into most of the visible light region. S170 displays a kink in the curve at approximately 380 nm and continues to absorb in the visible region but lesser than the former powders. S200 shows

typical absorption edge of TiO_2 anatase which absorbs strongly in the UV region albeit exhibiting some tailing from 400 nm into 700 nm.

3.3 XPS analysis

XPS study was also performed to probe the dopant species and concentration. All peaks were callibrated to carbon C 1s peak at 284.6 eV (adventitious carbon). Figure 4 illustrates the high resolution spectras of elements present in the samples nitrogen (Figure 4a), oxygen (Figure 4b) and titanium (Figure 4c). Similar to diffuse reflectance UV-Vis absorption results shared previously, samples S100, S130 and S160 displayed comparable high resolution spectra profiles for all the elements. It can be inferred that the bond nature of all the elements are alike in these 3 samples. Nitrogen was detected at a concentration of 4 at%, and the N 1s signal is centered at 401.6 eV. The N1s peak position for $TEAH^+$ is quite close at 401.2 eV. Alternatively, the N 1s peak at 401.3 eV was attributed to Ti-O-N bonding by Prokes et al. in a similar preparative approach using TEA as the N dopant [37]. This suggests the presence of surface-bond chromophore [32].

Obvious changes in the elemental profiles of S170 was observed. O 1s and Ti 2p peaks were oberved to have shifted to lower binding energy and narrowed in peak width. Co-relating the XPS results with previous XRD analysis, we believe that nitrogen is mostly present within the titanate phase. The absense of nitrogen and differences in peak positions and broadening is due to the transition whereby the dual phase material undergoes major phase change from titanate-rich to anatase-rich composition supported by other chacterization described earlier. During the titanate transformation, nitrogen bonds were broken and the titanate structure is futher

destroyed to re-arrange into anatase thus resulting in the changes in binding energy; presenting S170 as an intermediate structure whereby phase transformation is incomplete.

3.4 BET analysis

BET technique was employed to measure the surface areas and pore size distribution of the as-synthesized samples (Figure 5). High surface area is regularly suggestive of enhanced photocatalytic performances since it presents more active sites for photoreactions to take place upon. The surface area and average pore size are as summarized in Table 1.

Pure titanates typically have high surface areas ranging from 130 to 300 m^2/g [25, 26] whereas anatase samples tend to possess low surface areas ranging from 10 to less than 100 m^2/g [38, 39]. We also measured the surface area of P25 to be 51.4 m^2/g. Hence as far as estimating the phase content goes, a high surface area is indicative of more titanate being present and a low surface area suggests that more anatase is present. The results show that as the hydrothermal processing temperature increased, surface area gradually decreased, signifying the titanate phase decreases in phase ratio and the anatase phase increases accordingly. This can be explained by the fact that the titanate structure embodies water molecules within the interlayer; this structure collapses upon dehydration and the TiO_6 octahedras rearrange themselves to form the more stable anatase at higher temperatures [33]. The BET surface area and pore size distribution of the as-prepared samples strongly depend on the hydrothermal temperatures (Figure 5). It can be seen that all prepared samples show type IV sorption isotherms according to IUPAC classification, indicating the presence of mesopores (2-50 nm). The isotherm presents a typical hysteresis loop of type H2 for S100 and S130 samples, which is attributed to the difference in the adsorption and desorption mechanisms occurring in the “ink-bottle” pores. S100 and S130

displayed close to equal surface area and similar pore distribution, indicating that the samples did not undergo much transition at the low temperature range between 100 to 130 °C. Both samples are titanate rich and the phase contents should be approximately the same. As the hydrothermal temperature increases, the hysteresis loops shift toward higher relative pressure and the area of the hysteresis loops gradually decrease, indicating the decrease of BET surface area and pore volume. Also, the peak of pore size distribution shifts toward larger pore diameter. The peak of pore diameter distribution below 10 nm is attributed to the nanogaps inside the nanoparticle, while the large pore diameter (> 10 nm) is due to the aggregation of as-prepared particles. The surface area for S160 decreased to 179.7 m^2/g, demonstrating a significant transition from dominating titanate phase to more anatase phase emerging. Upon further increase of the hydrothermal temperature to 170 and 200 °C, the hysteresis loop shift to high relative pressure and the loop shape changes from the type H2 to type H3, reflecting the appearance of the macrospore structures. The trend continues as surface area of S170 and S200 decreased to 121.9 m^2/g and 75.1m^2/g. In particular, S200 displays higher surface area than P25.

3.5 Adsorption performance of MB

Figure 6 compares the change in concentration (C) of MB under the dark across samples S100, S130, S160, S170, S200, P25 and blank MB solution. All concentrations were normalized to initial concentration (C_0). P25 shows little or no dark response, indicating poor adsorption of MB molecules onto its surface. Similarly S200, which was found to be anatase TiO_2 also shows little adsorption. The result is typical of TiO_2 materials which are known to adsorb poorly[34]. The dual phase samples show progressive improvement in adsorbing MB with increase in hydrothermal heating temperature. This is attributed to strong adsorption originating from the

titanate phase which is reported to adsorb organic species well [25, 40-42]. S160 fared the best in adsorption over all the other samples. In a study relating synthesis temperature on the dye adsorption of titanate nanotubes, Chung et al. discovered that the adsorption capacity of nanotubes increased for two basic dyes (BG5 and BV10) with increase in synthesis temperature [29, 43]. The MB concentration level using S160 dropped rapidly in the first hour and eventually tunnelled out, suggestive of an adsorption isotherm to saturation. S170 showed some adsorption but lower than the other samples. This observation can be correlated to its structure whereby most of the titanate phase underwent a transformation into anatase hence the decrease in adsorption completely for S200.

As the adsorption performance of S160 was evidently the best, it is interesting to understand the kinetics behind its unique activity. An adsorption isotherm of S160 was plotted across MB concentrations ranging from 0 to 20 mg L^{-1}. Figure 7 presents the adsorption isotherm of S160. The adsorption isotherm curve was fitted to well-known Freundlich and Langmuir adsorption models which are described as

Freundlich: $q = K_F C^{\frac{1}{n}}$ (1)

Langmuir: $q = \frac{q_m KC}{1+KC}$ (2)

where q (mg g^{-1}) is the amount of adsorbed MB, C the concentration of MB at equilibrium, q_m (mg g^{-1}) the maximum adsorption capacity, K_F and n are Freundlich constants and K is the Langmuir constant. The amount of MB adsorbed onto the photocatalyst q can be given by:

$$q = \frac{(C_0 - C_f)V}{M} \quad (3)$$

where C_0 and C_f represent the initial and final concentrations of MB in the solution, V is the volume of MB solution (L) and M is the mass of photocatalyst added (g). The Freundlich and Langmuir models can be linearised as:

Freundlich: $lnq = lnK_F + \left(\frac{1}{n}\right) lnC$ (4)

Langmuir: $\frac{1}{q} = \frac{1}{q_m KC} + \frac{1}{q_m}$ (5)

The Langmuir model describes monolayer adsorption whereas the Freundlich model describes a heterogeneous surface binding. The results of fitting can be seen in Table 2. A relatively high regression coefficient (R^2) is an indicator that the model successfully describes the kinetics of adsorption [44]. The Langmuir adsorption model was found to fit S160 reasonably well where R^2 value was found to be closer to unity. The value of q_m derived theoretically was also in close agreement to the experimental value. Hence, the adsorption of MB is determined as monolayer adsorption; whereby a layer of MB molecules form over the surface of dual phase S160. The MB adsorbed for S160 (q_m) was found to be 162.19 mg/g and fared comparatively higher in adsorption as compared to other reported adsorbents such as rice husk (40.58 mg/g)[45]], raw date pits (80.29 mg/g)[3] and titanate nanotubes (133.33 mg/g) [25].

3.6 Photocatalytic degradation of MB under visible light

Figure 8 shows the photocatalytic activity of MB decomposition under visible light irradiation. A filter was used to cut off all wavelengths under 420 nm thus exposing only visible light.

Once more, S160 shows the best activity; nearly all the MB disappears in 6 hours. As discussed above, S160 was found to be successfully sensitized with nitrogen and nitrogen-

complex for visible light absorption. Although the surface area of this sample was not the highest among all samples, it had the best combination of high surface area and improved crystallinity which contributes to less defect states that promote electron hole recombination. In addition, the intimately matched interfaces of titanate and anatase on nanoscale promote charge transfer that further reduces electron hole recombination. Blank MB shows some decomposition under visible light which is due to the effect of direct photolytic breakdown of MB [46]. P25 does not demonstrate much visible light activity since both the anatase and rutile phases within the sample absorbs only in the UV region. The weak photo-activity shown is presumably a result of photolysis or dye sensitization effect which is lesser than that of blank MB due to suspended P25 particles blocking the penetration of light into the solution. Pure anatase S200 displayed a similar trend line, its poor surface adsorption does not facilitate in the photo-degradation process. In addition, pure anatase absorbs little visible light; hence there is little marked improvement in MB decomposition. S100 showed little improvement over blank MB irradiation, likely due to the poorly crystalline phases which contain defect sites that trap electrons and holes formed to impede the degradation rate. Comparatively, S170 and S130 fared much better under visible light irradiation. S130 showed approximately 60% decrease in MB concentration. Its visible light degradation performance is a result of successful nitrogen inclusion in the titanate phase. S170 demonstrated approximately 50% decrease in concentration. As discussed in the previous section, S170 is an intermediate structure due to incomplete transformation from titanate to anatase phase. It is presumed that the interfaces remain intimately matched during this transformation and aid in electron-hole separation that forms from excitation of the dye under visible light.

The kinetics of MB degradation is presented in Figure 9 by plotting the logarithm of the normalized dye concentration against irradiation time. Fairly good linear relationships were

observed thus establishing the degradation to follow a modified Langmuir-Hinshelwood mechanism:

$$\frac{dC}{dt} = \frac{k_r K_e C}{1 + k_e C} \quad (6)$$

Expressed in integral form it gives:

$$t = \frac{1}{K_e k_r} In \frac{C}{C_0} + \frac{1}{k_r}(C_0 - C) \quad (7)$$

When the concentration of the dye is adequately low (<< 10^{-3}) as is the condition of the experiment, the equation can be expressed as:

$$In \frac{C}{C_0} = k_r K_e t = k' t \quad (8)$$

where C and C_0 represent the concentration of MB at time t and initial concentration, k_r is the apparent reaction rate constant, K_e is the apparent equilibrium constant for the dye to adsorb onto the photocatalyst and k' represents the overall rate constant.

The results show that degradation of all samples was well described by the pseudo first order kinetic model. All the linear plots have R^2 values close to unity. S160 shows a degradation rate constant k' of 0.63438, which is approximately 21 times that of P25 under visible light irradiation. The degradation curve for S160 (Figure 8) was less linear than its counterparts, which is indicative that the overall degradation over the sample could be influenced by synergistic adsorption and degradation reactions.

4. Conclusion

In this work, a study focusing on the variation of synthesis temperature on a low temperature solvothermal route was performed to investigate phase transformation of titanate to

anatase TiO_2 within a dual phase photocatalyst. Nitrogen was successfully incorporated into the samples, thereby enhancing visible light absorption. The sensitized dual phase samples displayed superior degradation of methylene blue under visible light as compared to un-sensitized samples and P25. The titanate phase also contributed to surface adsorption which improved the overall photocatalytic process. Adsorption isotherm, kinetics, and photocatalytic degradation experiments show that S160 has the best adsorption in dark and degradation under visible light of MB. This work provides a platform to the understanding and design of dual phase photocatalysts, which is helpful for the future development of more efficient photocatalyts for pollutant treatment using visible light.

Acknowledgements

Financial support from the Environment and Water Industry Programme Office (EWI) under the National Research Foundation (NRF) of Singapore (grant MEWR651/06/160) is gratefully acknowledged.

References

[1] A.G. Agrios, P. Pichat, J. Photochem. Photobiol. A - Chem., 180 (2006) 130-135.
[2] M.R. Hoffmann, S.T. Martin, W.Y. Choi, D.W. Bahnemann, Chem. Rev., 95 (1995) 69-96.
[3] F. Banat, S. Al-Asheh, L. Al-Makhadmeh, Process Biochemistry, 39 (2003) 193.
[4] S.K. Kansal, M. Singh, D. Sud, J. Hazardous Mater., 141 (2007) 581-590.
[5] G. Alsayyed, J.C. Doliveira, P. Pichat, J. Photochem. Photobiol. A - Chem., 58 (1991) 99-114.
[6] T.Y. Zhang, T. Oyama, A. Aoshima, H. Hidaka, J.C. Zhao, N. Serpone, J. Photochem. Photobiol. A - Chem., 140 (2001) 163-172.
[7] M.A. Henderson, Surf. Sci. Reports, 66 (2011) 185-297.
[8] Y. Taga, Thin Solid Films, 517 (2009) 3167-3172.
[9] Z. Jiang, Y. Tang, Q. Tay, Y. Zhang, O.I. Malyi, D. Wang, J. Deng, Y. Lai, H. Zhou, X. Chen, Z. Dong, Z. Chen, Advanced Energy Materials, (2013) doi: 10.1002/aenm.201300380.

[10] A. Fujishima, X.T. Zhang, D.A. Tryk, Surf. Sci. Reports, 63 (2008) 515-582.
[11] X. Chen, S.S. Mao, Chem. Rev., 107 (2007) 2891-2959.
[12] A.L. Linsebigler, G.Q. Lu, J.T. Yates, Chem. Rev., 95 (1995) 735-758.
[13] X. Chen, L. Liu, P.Y. Yu, S.S. Mao, Science, 331 (2011) 746-750.
[14] Y. Tang, P. Wee, Y. Lai, X. Wang, D. Gong, P.D. Kanhere, T.-T. Lim, Z. Dong, Z. Chen, The J. Phy. Chem. C, 116 (2012) 2772-2780.
[15] Z.Y. Yuan, B.L. Su, Colloids and surfaces A: Physiochem. Eng Aspects, 241 (2004) 173.
[16] Y.B. Mao, S.S. Wong, J. Am. Chem. Soc., 128 (2006) 8217-8226.
[17] T. Kasuga, M. Hiramatsu, A. Hoson, T. Sekino, K. Niihara, Advanced Materials, 11 (1999) 1307.
[18] M.D. Hernandez-Alonso, F. Fresno, S. Suarez, J.M. Coronado, Energy & Environmental Science, 2 (2009) 1231-1257.
[19] J.C. Zhao, C.C. Chen, W.H. Ma, Topics in Catalysis, 35 (2005) 269-278.
[20] Q. Chen, W. Zhou, G. Du, L.M. Peng, Advanced Materials, 14 (2002) 1208.
[21] D.V. Bavykin, J.M. Friedrich, F.C. Walsh, Advanced Materials, 18 (2006) 2807-2824.
[22] T. Sasaki, K.M. Yu, Y. Fujiki, Chem. Mater., 4 (1992) 894-899.
[23] H. Irawa, S. Klkkawa, M. Koirunj, J. Phys. Chem., 86 (1982) 5023.
[24] X.M. Sun, Y.D. Li, Chemistry - A European Journal, 9 (2003) 2229-2238.
[25] L. Xiong, Y. Yang, J. Mai, W. Sun, C. Zhang, D. Wei, Q. Chen, J. Nia, Chem. Eng. Journal, 156 (2010) 313.
[26] Y.W.L. Lim, Y. Tang, Y.H. Cheng, Z. Chen, Nanoscale, 2 (2010) 2751-2757.
[27] Y.X. Tang, Y.K. Lai, D.G. Gong, K.H. Goh, T.T. Lim, Z.L. Dong, Z. Chen, Chemistry - A European Journal, 16 (2010) 7704-7708.
[28] Y. Tang, D. Gong, Y. Lai, Y. Shen, Y. Zhang, Y. Huang, J. Tao, C. Lin, Z. Dong, Z. Chen, J. Mater. Chem., 20 (2010) 10169-10178.
[29] C.K. Lee, S.S. Liu, L.C. Juang, C.C. Wang, M.D. Lyu, S.H. Hung, J. Hazardous Mater., 148 (2007) 756.
[30] E. Morgado, P.M. Jardim, B.A. Marinkovic, F.C. Rizzo, M.A.S. De Abreu, J.L. Zotin, A.S. Araujo, Nanotechnology, 18 (2007).
[31] Y. Guo, N.H. Lee, H.J. Oh, C.R. Yoon, K.S. Park, W.H. Lee, Y. Li, H.G. Lee, K.S. Lee, S.J. Kim, Thin Solid Films, 516 (2008) 8363-8371.

[32] Y.H. Cheng, V.P. Subramaniam, D.G. Gong, Y.X. Tang, J. Highfield, S.O. Pehkonen, P. Pichat, M.K. Schreyer, Z. Chen, J. Solid State Chem., 196 (2012) 518-527.
[33] Y.H. Cheng, Y.Z. Huang, P.D. Kanhere, V.P. Subramaniam, D.G. Gong, S. Zhang, J. Highfield, M.K. Schreyer, Z. Chen, Chemistry - A European Journal, 17 (2011) 2575-2578.
[34] A. Mills, J.S. Wang, J. Photochem. Photobiol. A - Chem., 127 (1999) 123-134.
[35] J.L. Gole, J.D. Stout, C. Burda, Y.B. Lou, X.B. Chen, J. Phy. Chem. B, 108 (2004) 1230-1240.
[36] C. Burda, Y. Lou, X. Chen, A.C.S. Samia, J. Stout, J.L. Gole, Nano Letters, 3 (2003) 1049.
[37] S.M. Prokes, J.L. Gole, X. Chen, C. Burda, W.E. Carlos, Adv. Func. Mater., 15 (2005) 161.
[38] C.C. Wang, J.Y. Ying, Chem. Mater., 11 (1999) 3113.
[39] M. Toyoda, Y. Nanbu, Y. Nakazawa, M. Hirano, M. Inagaki, Applied Catalysis B: Environmental, 49 (2004).
[40] Q. Li, T. Kako, J. Ye, Applied Catalysis A: General, 375 (2010) 85.
[41] K.V. Baiju, S. Shukla, S. Biju, M.L.P. Reddy, K.G.K. Warrier, Materials Letters, 63 (2009) 923-926.
[42] Y. Tang, Z. Jiang, Q. Tay, J. Deng, Y. Lai, D. Gong, Z. Dong, Z. Chen, RSC Advances, 2 (2012) 9406-9414.
[43] C.K. Lee, K.S. Lin, C.F. Wu, M.D. Lyu, C.C. Lo, J. Hazardous Mater., 150 (2008) 494.
[44] M.M. El-Halwany, Desalination, 250 (2010) 208.
[45] V. Vadivelan, K.V. Kumar, J. Colloid Inter. Sci., 286 (2005) 90.
[46] Y. Zhao, X. Qiu, C. Burda, Chem. Mater., 20 (2008) 2629-2636.

Figures and Captions

Figure 1: X-Ray diffraction patterns of samples treated at various temperatures (a) S100, (b) S130, (c) S160, (d) S170 and (e) S200. T denotes titanate and A denotes anatase phases.

Figure 2: TEM images of (a) S100, (b) S160, and (c) S200 samples.

Figure 3: (a) Visual comparison of as synthesized powders, and (b) Diffuse reflectance spectroscopy curves displaying absorbance of corresponding powders.

Figure 4: High resolution XPS spectrums of (a) nitrogen N1s, (b) oxygen O1s and (c) titanium Ti 2p for samples S100, S130, S160, S170 and S200.

Figure 5: (a) Adsorption and desorption curves; (b) BJH desorption curves showing the pore volume distribution.

Figure 6: Adsorption of methylene blue under dark using photocatalyst samples P25, S100, S130, S160, S170 and S200.

Figure 7: Adsorption isotherm of S160 sample.

Figure 8: Photocatalytic degradation of methylene blue under visible light (> 420 nm) using samples P25, Blank MB solution, S100, S130, S160, S170 and S200.

Figure 9: First order degradation rates for P25, Blank MB, S100, S130, S160, S170 and S200 under visible light irradiation.

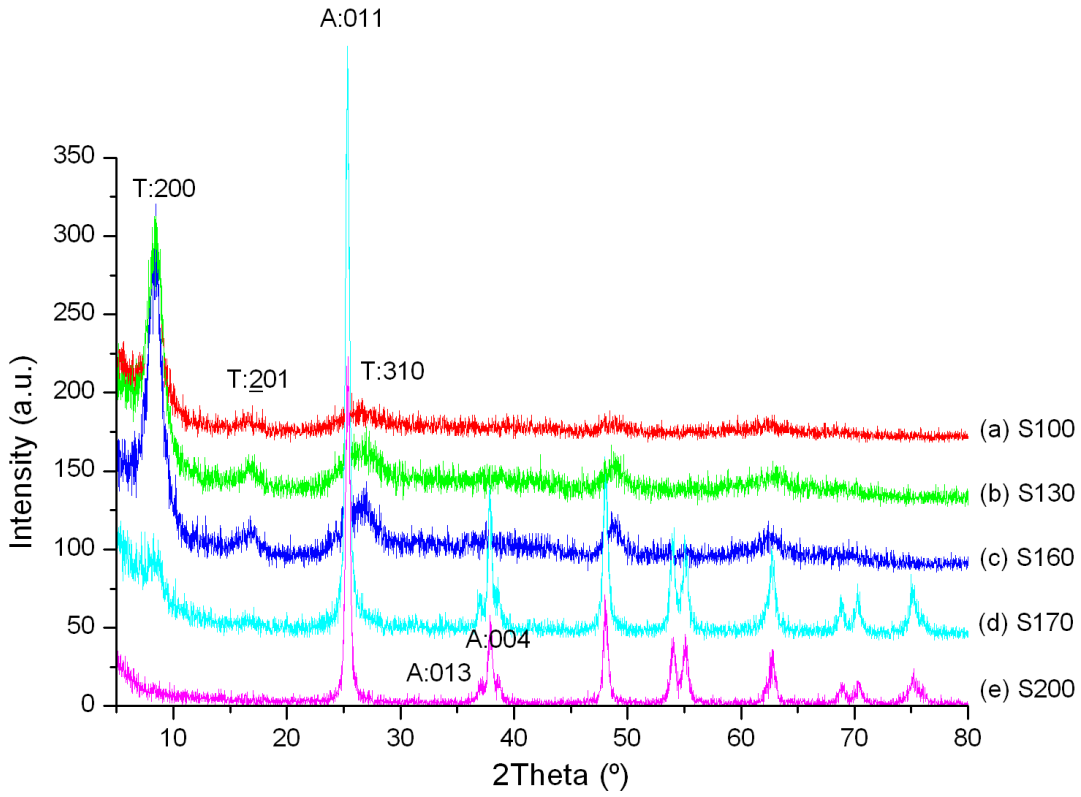

Figure 2: X-Ray diffraction patterns of samples treated at various temperatures (a) S100, (b) S130, (c) S160, (d) S170 and (e) S200. T denotes titanate and A denotes anatase phases.

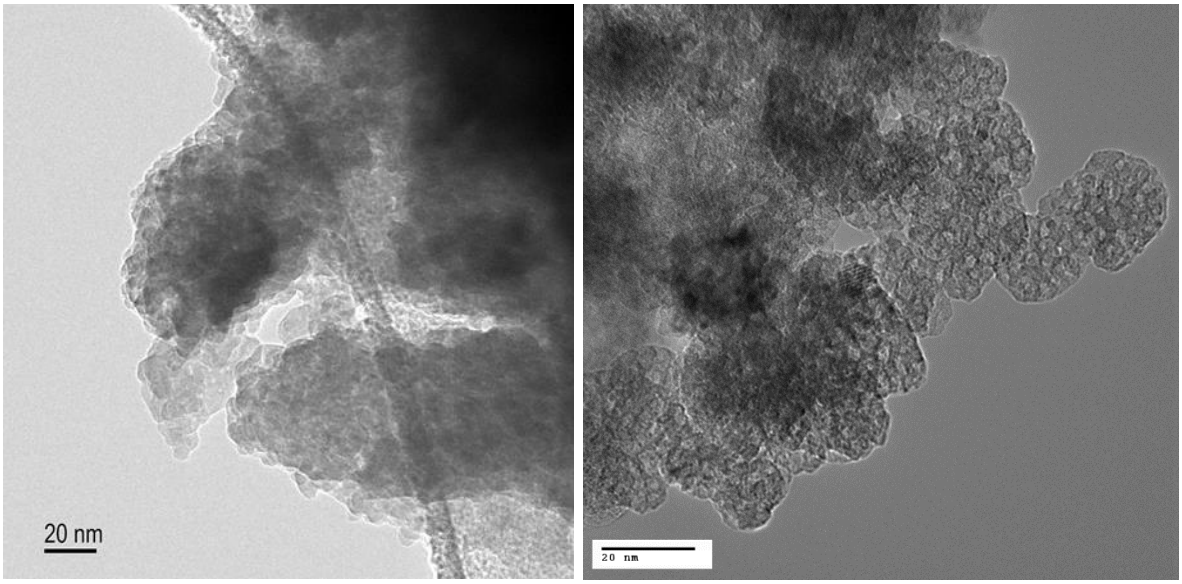

(a) (b)

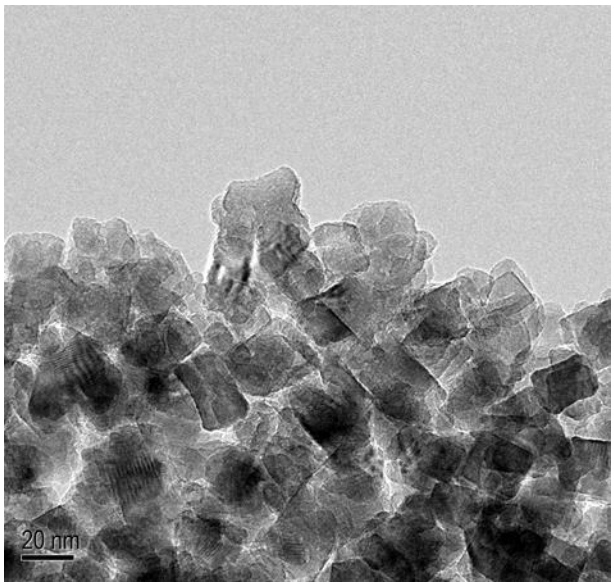

(c)

Figure 2: TEM images of (a) S100, (b) S160, and (c) S200 samples.

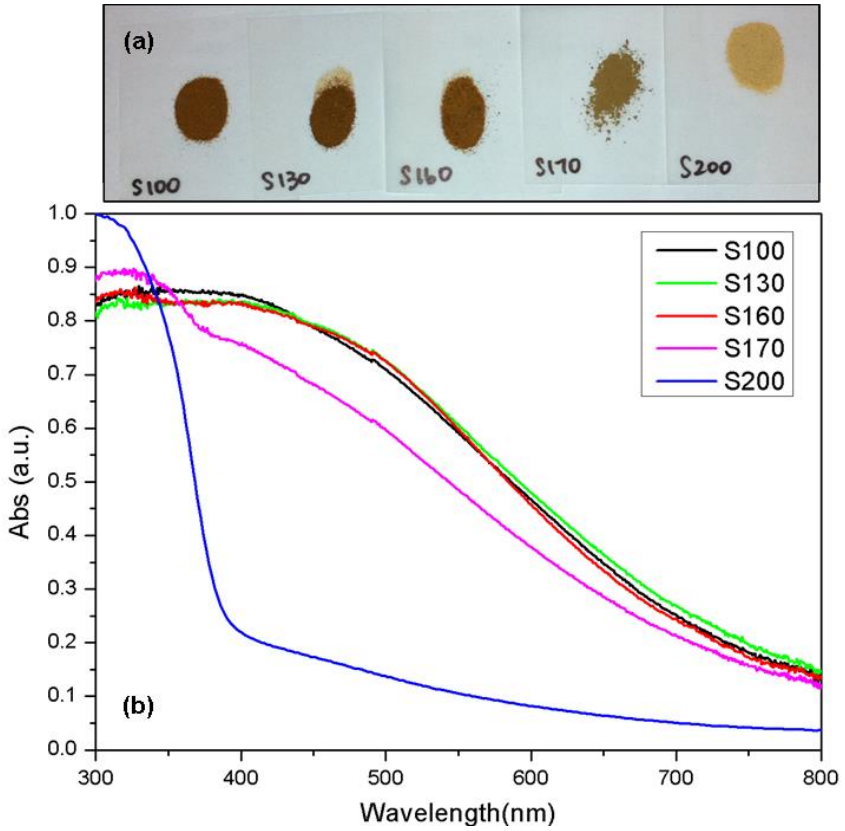

Figure 3: (a) Visual comparison of as synthesized powders, and (b) Diffuse reflectance spectroscopy curves displaying absorbance of corresponding powders

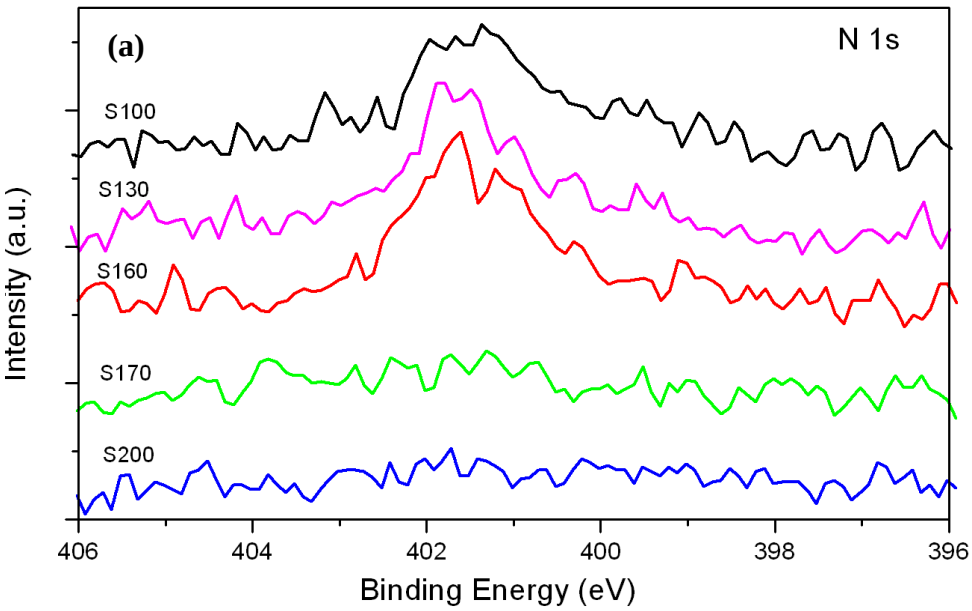
(a)
N 1s
S100
S130
S160
S170
S200
Intensity (a.u.)
406
404
402
400
398
396
Binding Energy (eV)

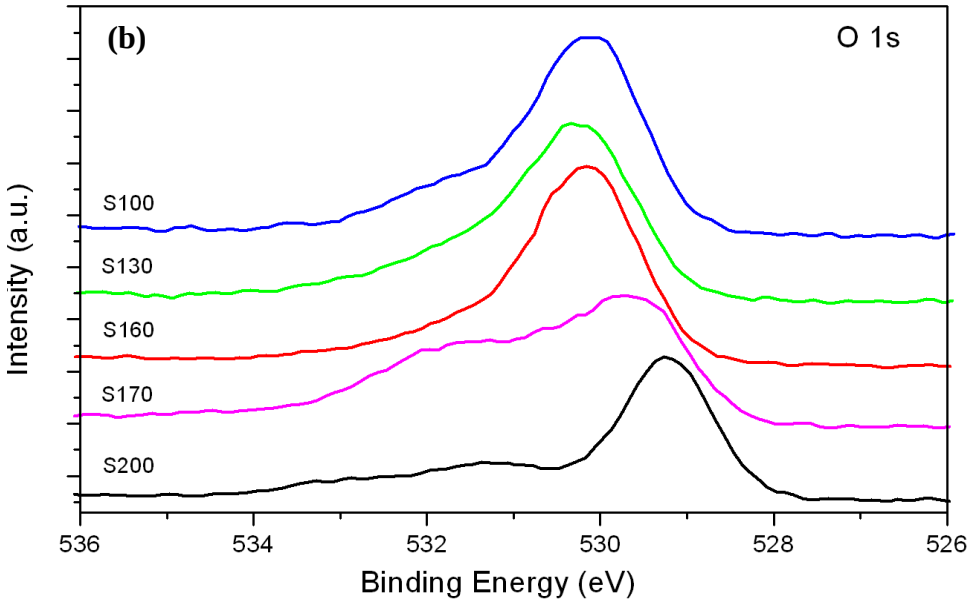
(b)
O 1s
S100
S130
S160
S170
S200
Intensity (a.u.)
536
534
532
530
528
526
Binding Energy (eV)

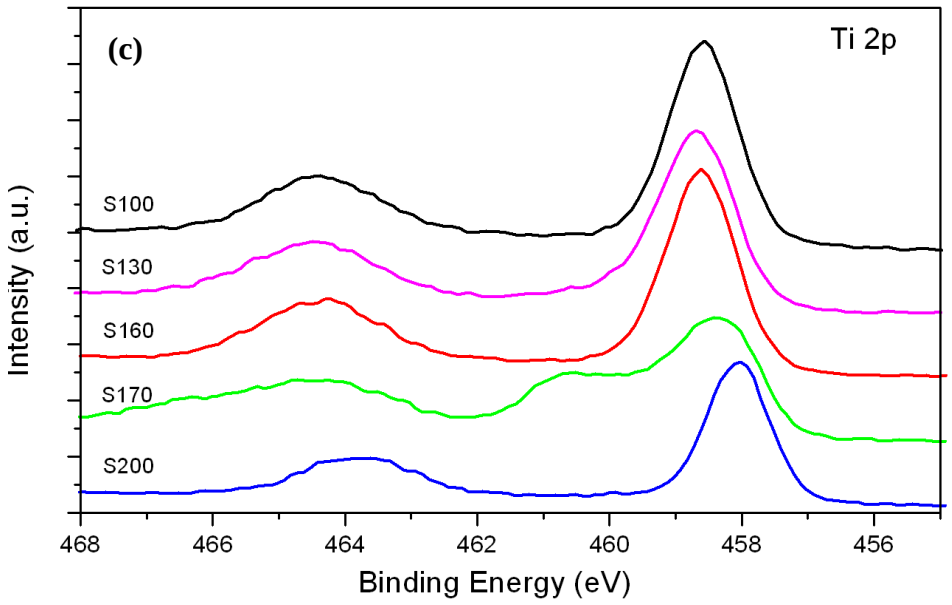

Figure 4: High resolution XPS spectrums of (a) nitrogen N1s, (b) oxygen O1s and (c) titanium Ti 2p for samples S100, S130, S160, S170 and S200.

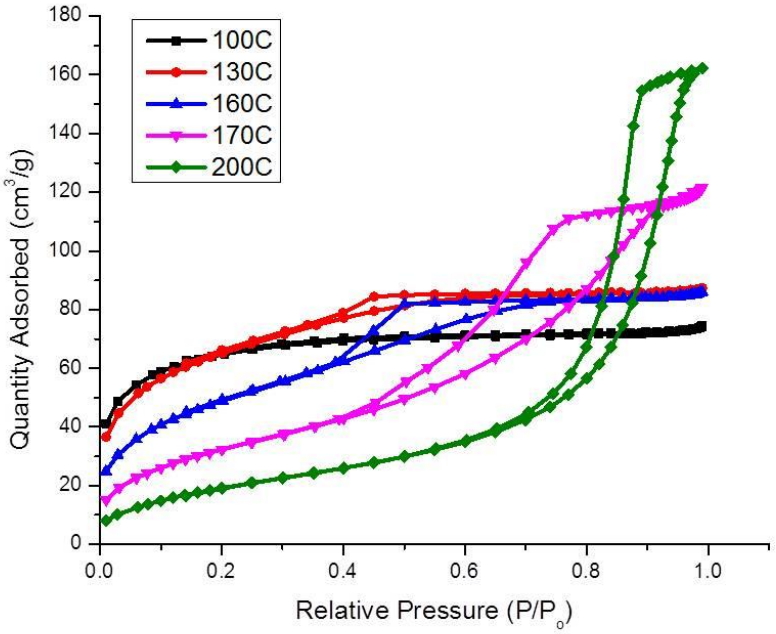

(a)

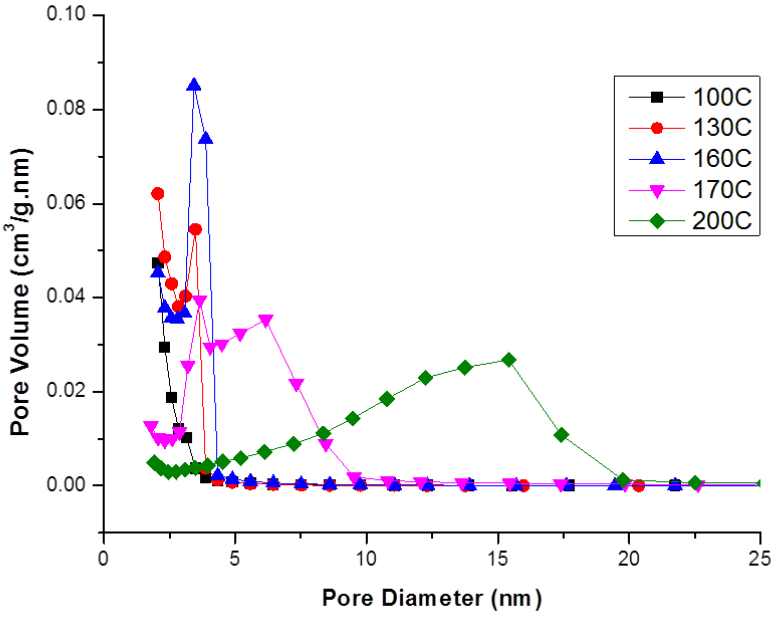

(b)

Figure 5: (a) Adsorption and desorption curves; (b) BJH desorption curves showing the pore volume distribution.

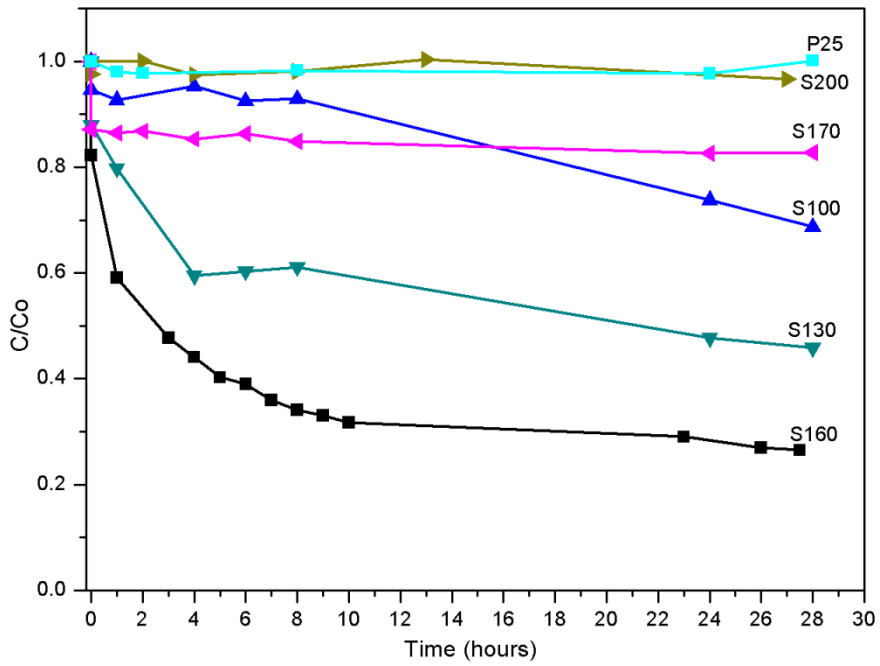

Figure 6: Adsorption of methylene blue under dark using photocatalyst samples P25, S100, S130, S160, S170 and S200.

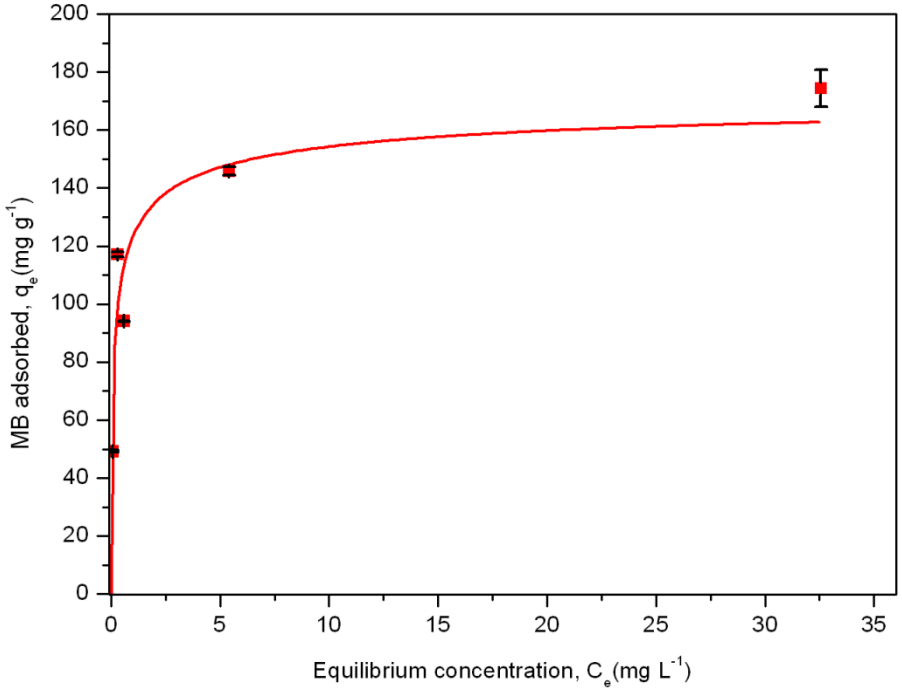

Figure 7: Adsorption isotherm of S160 sample

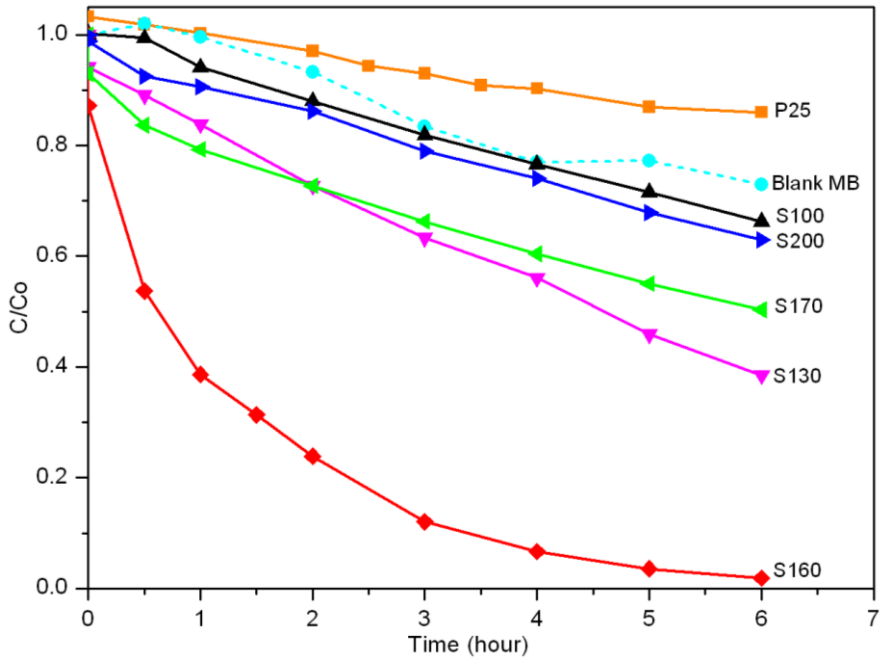

Figure 8: Photocatalytic degradation of methylene blue under visible light (> 420 nm) using samples P25, Blank MB solution, S100, S130, S160, S170 and S200.

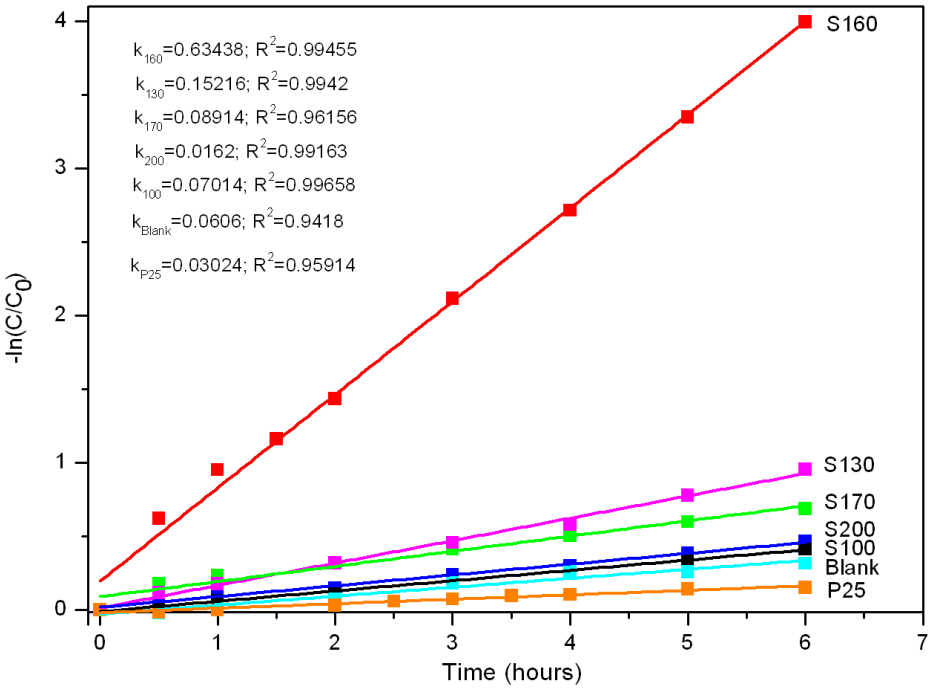

Figure 9: First order degradation rates for P25, Blank MB, S100, S130, S160, S170 and S200 under visible light irradiation.